Measurement of strong phonon softening in Cr with and without Fermi-surface nesting by inelastic x-ray scattering

D. Lamago,[1,2] M. Hoesch,[3] M. Krisch,[3] R. Heid,[1] K.-P. Bohnen,[1] P. Böni,[4] and D. Reznik[1,5]
[1]*Karlsruher Institut für Technologie, Institut für Festkörperphysik, P.O. Box 3640, D-76021 Karlsruhe, Germany*
[2]*Laboratoire Léon Brillouin, CEA Saclay, F-91191 Gif-sur-Yvette, France*
[3]*European Synchrotron Radiation Facility, F-38043 Grenoble Cedex, France*
[4]*Physik Department E21, Technische Universität München, D-85748 Garching, Germany*
[5]*Department of Physics, University of Colorado–Boulder, Boulder, Colorado 80309, USA*
(Received 22 July 2010; published 15 November 2010)

Nesting of the Fermi surface can soften and broaden phonons at the nesting wave vectors. However, huge electron-phonon anomalies unexpected from the experimental topology of the Fermi surface have been reported in copper oxide superconductors and their origin remains enigmatic. Here we present results of inelastic x-ray scattering measurements that uncovered similarly pronounced softening of phonons in chromium that occur far from the nesting wave vectors of the Fermi surface. The softening appears in addition to the previously reported phonon anomalies at the nesting wave vectors. Calculations in the local-density approximation show that the anomalies result from the enhancement of the electron-phonon coupling constant. Our results demonstrate that strong electron-phonon coupling alone can result in strong phonon anomalies limited to a small range of wave vectors. They imply that the phonon anomalies in copper oxide superconductors may be explained by an enhanced electron-phonon coupling strength without invoking novel collective modes or some hidden nesting of the Fermi surface.

DOI: 10.1103/PhysRevB.82.195121 PACS number(s): 75.30.Fv, 71.38.−k, 71.45.Lr, 78.70.Ck

I. INTRODUCTION

In metals with Fermi surfaces, phonons may couple to singularities in the electronic density of states, which appear at so-called nesting wave vectors, which connect parallel (nested) sheets of the Fermi surface.[1] This nesting greatly enhances the number of possible electronic transitions at the nesting wave vectors compared to other wave vectors, which results in softer and broader phonons. These singularities can produce sharp features in phonon dispersions called Kohn anomalies. Classic examples of this behavior are pronounced phonon-dispersion dips at $2k_f$ (k_f is the Fermi momentum) in one-dimensional conductors where one dimensionality of the electronic states leads to the Fermi-surface nesting at $2k_f$.[2] It was noticed early on that Fermi-surface nesting alone cannot adequately explain phonon softening resembling Kohn anomalies in many cases. For example, dispersions of certain phonons in NbC and TaC dip relatively sharply and strongly at wave vectors where the Fermi-surface nesting is present but is relatively weak. Wave-vector ($\mathbf{q}$) dependence of electron-phonon coupling strength combined with nesting has been invoked to explain the strength of such phonon anomalies.[3–5]

Strong electron-phonon effects similar to Kohn anomalies have been observed in cuprate superconductors[6] but photoemission experiments do not show any features in the electronic band structure or the Fermi surface that may enhance the number of possible electronic transitions at the anomalous wave vector. Possible explanations of this phonon renormalization are in terms of phonons interacting with a collective mode, e.g., related to stripe order, some kind of hidden nesting of the Fermi surface, or in terms of extremely strong electron-phonon coupling (matrix element) at the anomalous wave vector. The latter possibility seems to be rather far fetched since phonon anomalies that are not at all associated with either nesting or interactions with collective modes have never been reported. We show that in Cr the observed strong phonon renormalization limited to specific wave vectors originates from enhanced electron-phonon coupling alone for most anomalous phonons.

Cr is one of the most famous materials exhibiting incommensurate order. Although Cr crystallizes in a simple bcc structure, its Fermi surface exhibits a rather complicated shape. As first pointed out by Lomer,[7] a spin-density wave (SDW) occurs due to the nesting of the "jack-shaped" electron Fermi surface at the Γ point (0,0,0) with the octahedral-shaped hole surface at the H point (1,0,0). At the Néel temperature T_N=311 K, Cr undergoes a transition to a transversely polarized SDW (TSDW) at an incommensurate wave vector $\mathbf{Q}^{\pm}=(1\pm\delta,0,0)$, where $\delta\approx 0.048$. At T_{sf} =121 K, a first-order phase transition takes place from the TSDW phase to a longitudinally polarized SDW (LSDW) phase with the same modulation vector, where the moments are oriented along $\mathbf{Q}^{\pm}$.

The magnetic excitation spectrum in Cr also exhibits many unusual features. In the LSDW phase, incommensurate excitations with longitudinal and transverse polarization with respect to the staggered magnetization emerge from the magnetic satellite peaks with an extremely steep dispersion on the order of 1000 meV Å. In addition, diffuse scattering evolves in the region between the satellite positions and becomes stronger with increasing temperature and energy. Most remarkably, additional low-energy modes with longitudinal polarization appear (Fincher-Burke modes) above T_{sf} in the TSDW phase. While the incommensurate excitations can be essentially explained in terms of the three-band model,[8] the nature of the Fincher-Burke modes is not yet understood.[9,10]

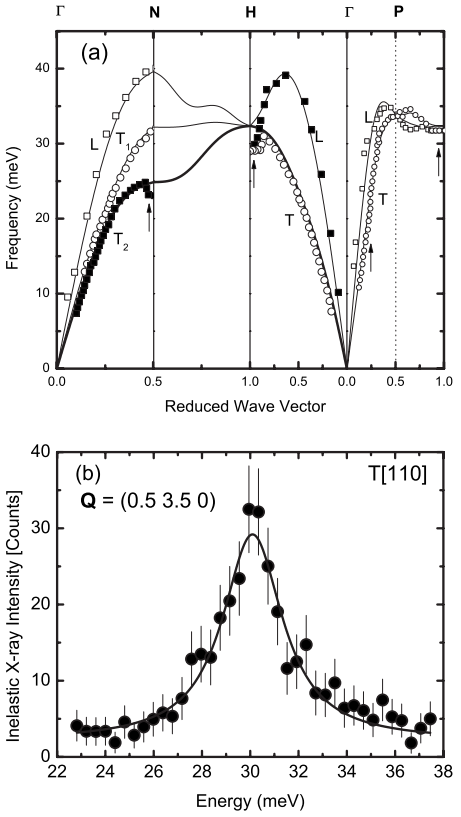

FIG. 1. (a) Phonon dispersion as calculated by means of the Born-von-Karman model along the high-symmetry directions. Data points represent previous neutron data (Ref. 15). Arrows indicate anomalies as observed by neutron scattering (Ref. 15). Branches of interest here are shown in bold. (b) Raw data from inelastic x-ray scattering as function of energy transfer at $T=320$ K and $\mathbf{Q}=(0.5,3.5,0)$. The solid line corresponds to a fit to the data using a Lorentzian.

Associated with the SDW, there is a distortion of the lattice with twice δ. Charge-density waves (CDWs) were observed there using synchrotron radiation[11] confirming previous results by x-ray[12] and neutron diffraction.[13] In addition, higher harmonics of the SDW as well as the CDW were observed. The occurrence of the CDW can be either explained in terms of Fermi-surface nesting[14] or by a strain wave induced by the magnetoelastic coupling to the SDW.

Interaction of the conduction electrons with the lattice vibrations enhanced by the Fermi-surface anomalies such as nesting leads to anomalous phonon dispersions at wave vectors of extremal dimensions of the Fermi surface (Kohn anomalies). Using inelastic neutron scattering (INS), Shaw and Muhlestein[15] identified four regions of anomalous transverse phonon softening in Cr, which they associated with the topology of the Fermi surface. Their experimental data are reproduced in Fig. 1, which shows transverse (T) and longitudinal (L) acoustic-phonon branches. There are two transverse-acoustic branches in the [110] direction, T1 and T2. The most pronounced anomalies appear near the H point and the N point as softening of the measured frequencies at positions marked by arrows. The relatively poor wave-vector (**Q**) resolution, however, washed out the phonon anomalies, thus precluding a direct comparison of the anomalous wave vectors with the position of the magnetic peaks.

Our goal was to determine whether or not there is a correspondence between phonon anomalies and the Fermi-surface nesting in Cr. To improve the **Q** resolution over the previous INS study,[15] which covered only the high-symmetry directions, we used inelastic x-ray scattering (IXS). We investigated the phonon dispersion near the H point and extended the measurements along the zone boundary to the N point where another phonon anomaly occurs. Experimental results were then compared with our calculations of both phonon anomalies and the Fermi-surface nesting. Our main finding was a clear observation of strong phonon softening in a narrow **q** range far from any nesting wave vectors, the first from any metal aside for the high-T_c cuprates.

II. EXPERIMENTAL DETAILS

The IXS experiments were performed at the ESRF on the ID-28 beam line using (9 9 9) Si reflections, providing an energy resolution of 3 meV full width at half maximum (FWHM). The sample was a high-quality single crystal of Cr in the "multi-**Q**" state with magnetic ordering observed along all equivalent [100] directions. It was mounted in a closed-cycle refrigerator with the temperatures varying between 50 and 320 K. We measured phonon frequencies in the Brillouin-zone (BZ) centered at the $\mathbf{Q}=(3,1,0)$ reciprocal-lattice position, where the structure factor of the anomalous phonons is maximized. The zone boundary was at $\mathbf{Q}=(3,0,0)$ in the [100] direction and at $\mathbf{Q}=(3,0.5,0.5)$ in the [110] direction. Moving between these two positions along the zone boundary, the [110] T2 branch connects to the [100] T branch [Fig. 1(a)]. This made it possible to investigate the phonon anomaly along the entire two-dimensional cut through the BZ without the restriction of the high-symmetry directions. Figure 1(b) shows an example of raw data at $\mathbf{Q}=(0.5,3.5,0)$ corresponding to the [110] T2 branch and fitted with a Lorentzian. The blue lines marked by small letters in Fig. 2(a) show the positions in reciprocal space along which we measured the phonon frequencies.

III. EXPERIMENTAL RESULTS

The effects of electronic excitations across the Fermi surface on phonons can only be modeled by very long-range forces or extra attractively interacting shells if a shell model is used.[4] Thus, to isolate the effects of conduction electrons, we first compared the experimental dispersions with the Born-von-Karman model, which includes only short-range interatomic forces (up to second-nearest neighbors). Results of this model calculation with parameters fitted to previously published neutron data[15] are included in Fig. 1(a).

Figure 2 compares calculated and measured phonon dispersions along the lines in reciprocal space shown in Fig. 2(a). Figures 2(b) and 2(c) shows the IXS results where previous neutron measurements were conducted. We observe clear dispersion minima at $h=0.95$ in the [100] direction and at $h=0.5$ in the [110] direction. These results convincingly demonstrate that the position of the minimum of the phonon dispersion corresponds to the magnetic satellite peaks of the

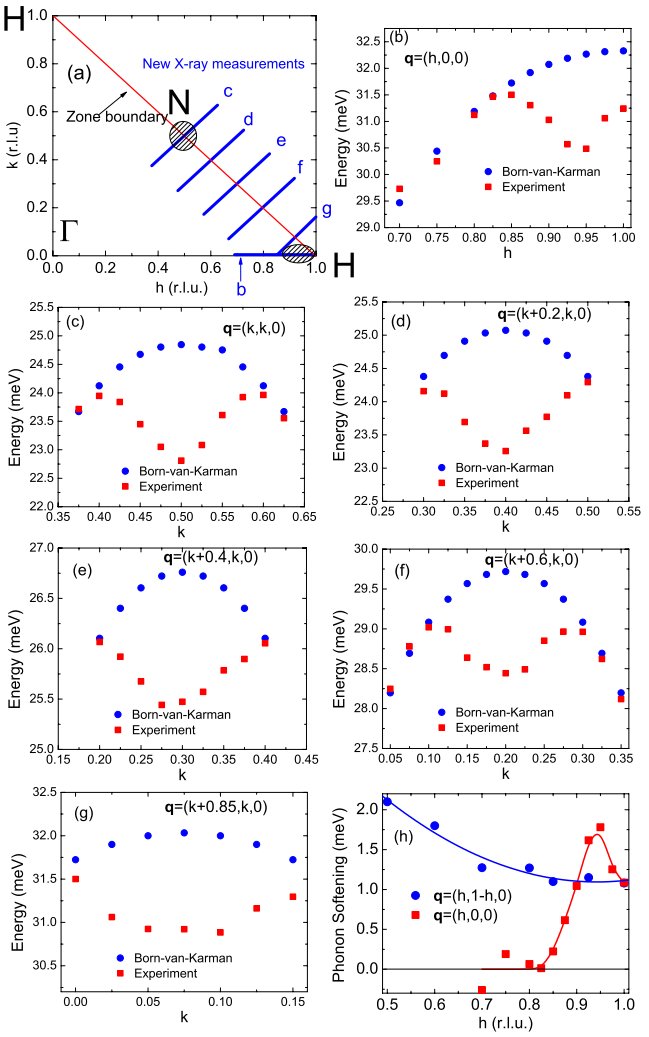

FIG. 2. (Color online) Comparison between experiment and Born-von-Karman calculations. The experiments were performed at $T=300$ K. (a) A schematic of the scans in reciprocal space. Hatched ovals indicate previously observed phonon anomalies; [(b)–(g)] calculated (blue circle) and measured (red square) phonon dispersions along the paths indicated in (a); (h) difference ($E_{calc}-E_{exp}$) between the calculated and experimental phonon dispersion along the zone boundary N-H (blue circle) and along the high-symmetry direction Γ-H (red square).

SDW. There was no change in the position or magnitude of the dip of the dispersion with temperature variation between 50 and 320 K. In particular, the dip survives in the paramagnetic phase. The only effect we have observed on cooling the sample to 50 K was the overall hardening of the phonon dispersion, which is consistent with extrapolating the results of Refs. 16 to lower temperatures.

We then investigated the evolution of the phonon anomaly between $\mathbf{q}=(0.5,0.5,0)$ and $\mathbf{q}=(1,0,0)$ [Figs. 2(d)–2(g)]. The experimental results as compared with the predictions of the Born-von-Karman model show that the phonon-dispersion minimum persists all along the zone-boundary line connecting the two wave vectors [between the N and H points in Fig. 1(a)]. Thus, anomalous phonon softening is not limited to the high-symmetry directions but extends along the zone boundary.

Figure 2(h) shows the difference between the Born-von-Karman model and the experimental values along the [100] direction (red) and along the zone boundary (blue). Along the [100] direction, the phonon softening has a distinct maximum at $\mathbf{q}=(0.94,0,0)$, the position of the SDW satellite as discussed above. The anomaly is also present along the entire zone-boundary line between $\mathbf{q}=(0.5,0.5,0)$ and $\mathbf{q}=(1,0,0)$. The strongest renormalization along this line is 2 meV at $\mathbf{q}=(0.5,0.5,0)$ and the weakest is 1 meV at $\mathbf{q}=(1,0,0)$. The linewidth of all phonons remains resolution limited (≤ 0.5 meV) within the experimental uncertainty at all q.

IV. DFT CALCULATIONS

To understand the mechanism behind these phonon anomalies we performed density-functional calculations of the lattice dynamics using the mixed-basis pseudopotential method and the linear-response technique.[17–19] In the construction of a Vanderbilt-type pseudopotential[20] for Cr, $3s$ and $3p$ semicore states were included in the valence space. The fairly localized semicore states are treated efficiently in the mixed-basis scheme employing a combination of local functions and plane waves for the representation of the valence states. Local s, p, and d orbitals had a radial cutoff of 2.1 bohrs, supplemented by plane waves up to a kinetic energy of 24 Ry. For the exchange-correlation functional the local-density approximation (LDA) in the parametrization of Perdew-Wang[21] was applied. We only considered nonmagnetic states. The present results are obtained for the optimized lattice constant of 2.788 Å, which shows the typical overbinding of LDA with respect to the experimental value of 2.88 Å. Brillouin-zone integrations were performed using $8\times8\times8$ k points in the irreducible wedge of the BZ (IBZ) in connection with a smearing technique employing a Gaussian broadening of 0.2 eV. The complete phonon dispersion was obtained by standard Fourier interpolation of the dynamical matrices calculated at 145 $\mathbf{q}$ points in the IBZ. These parameters guaranteed sufficient convergence of phonon frequencies except in the anomalous regions. Additional calculations with 22 960 k points in the IBZ and reduced broadenings of 0.1 and 0.05 eV have been performed for selected reduced momentum transfers $\mathbf{q}$ along [100] and [110]. The calculation along the high-symmetry directions [Figs. 3(a) and 3(b)] was performed with two different values of Fermi-surface smearing in order to determine the sensitivity of the phonon anomalies to the nesting. The calculations away from the high-symmetry directions were performed using a different numerical grid, which gave the same result at $\mathbf{q}=(0.5,0.5,0)$.

The color map in Fig. 4 shows the calculated joint density of states for electron-hole excitations at the Fermi surface, defined by $\chi''(\mathbf{q})=\Sigma_k\delta(\varepsilon_k-\varepsilon_F)\delta(\varepsilon_{k+q}-\varepsilon_F)$. In the calculation the δ functions were replaced by Gaussians with a width of 0.1 eV. There are two bright spots at $\mathbf{Q}^{\pm}$ away from the H point and weaker ones near the N point. These are the nesting features that have been previously held responsible for the phonon softening around the corresponding wave vectors.[15] However, there is no enhancement of the phase space for electronic excitations at the wave vectors of the

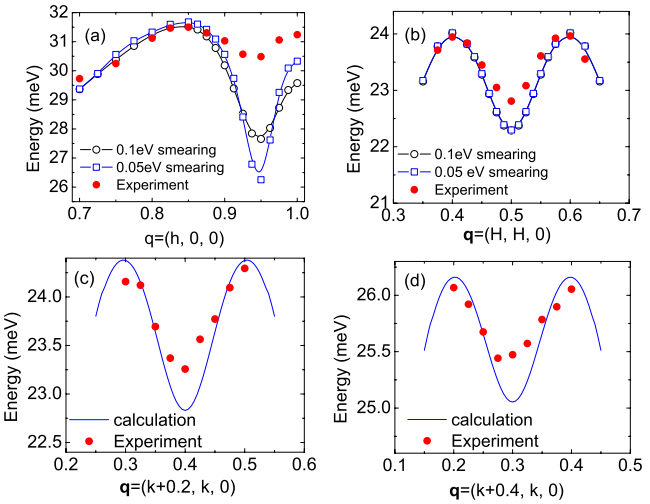

FIG. 3. (Color online) Comparison between phonon dispersions and the LDA calculation. [(a) and (b)] Black open circles represent a factor of two more smearing than the blue open squares. [(c) and (d)] Experiment and calculation away from the high-symmetry directions.

new set of phonon anomalies along the zone boundary $\mathbf{q}=(h,1-h,0)$ that we found [blue line through the round points in Fig. 2(h)]. This behavior seems to be analogous to the copper oxide superconductors[3] where a strong phonon anomaly near $\mathbf{q}=(0.3,0.0)$ is not associated with any enhanced joint density of states.

Three bands cross the Fermi surface [Fig. 5(a)] giving three intraband and three interband contributions to the phonon self-energy. Figures 5(b)–5(g) show calculated band-by-band contributions to both the phonon linewidth and to the joint density of states, which approximates the imaginary part of the susceptibility. The ratio of the two is the **q**-dependent electron-phonon coupling strength.

The features in the susceptibility along [110] are primarily due to transitions inside band 2. However, electron-phonon coupling enhances contributions of other bands to the phonon linewidth, particularly interband transitions between

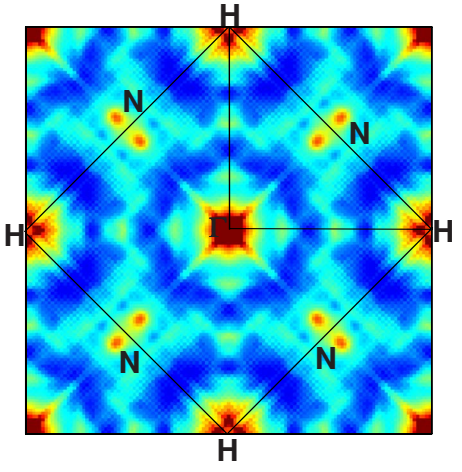

FIG. 4. (Color online) Joint density of states for electron-hole excitations, whose "hotspots" (in red) correspond to potential phonon anomalies.

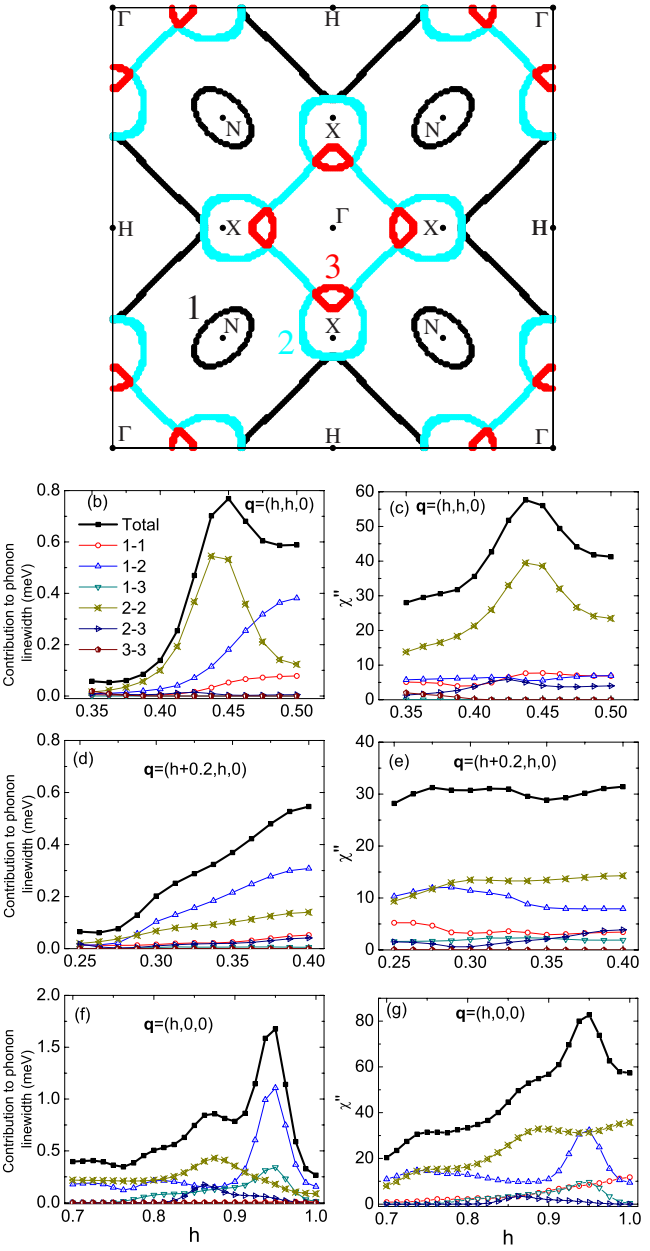

FIG. 5. (Color online) Interband and intraband contributions to the phonon linewidth and the electronic joint density of states (see Fig. 3). (a) Calculated (100)/(010) cut of the Fermi surface of Cr. Numbers (1,2,3) index the three bands crossing the Fermi surface that are referenced in the legend in (b). (b) and (c) show the contributions of the six relevant electronic transitions to the phonon linewidth and the imaginary part of the susceptibility, respectively, along the [110] direction. Similarly, (d) and (e) and (f) and (g) show the contributions along $\mathbf{q}=(h+0.2,h,0)$ and along the [100] direction, respectively. The legend in (b) applies to all graphs [(b)–(g)].

bands 1 and 2. As a result, the phonon self-energy has a very different **q** dependence, in particular, the interband contribution enhances it near the zone boundary and makes the susceptibility peak near 0.45 less pronounced. Remarkably, the calculated enhancement in the phonon linewidth at this wave vector does not correspond to any calculated or experimental feature in the phonon dispersion. Although it is widely be-

lieved that there should be a correspondence between the two, it was pointed out in Ref. 22 that this is not necessarily so. This peak at $h=0.45$ due to nested intraband transitions inside band 2 corresponds to the bright incommensurate spots near the N point in Fig. 4. These spots disappear as one moves along $\mathbf{q}=(h,1-h,0)$, thus the corresponding contribution from these intraband transitions should disappear as well. Indeed, Figs. 5(d) and 5(e) show that the intraband peak disappears from both the susceptibility and the phonon linewidth. On the other hand, the contribution to the linewidth from the transitions between bands 1 and 2 as well as the weaker contributions from the intraband transitions inside bands 1 and 2 that increase toward $\mathbf{q}=(0.5,0.5,0)$ remain at $\mathbf{q}=(0.6,0.4,0)$. Based on this evidence we conclude that these transitions are responsible for the observed dispersion dips at $(h,1-h,0)$.

Along [100] the main contributions to χ'' are also from interband transitions between bands 1 and 2 with a nesting wave vector at $\mathbf{q}=(0.95,0,0)$ as well as from the intraband transitions inside band 2, which show no strong $\mathbf{q}$-dependent features. [see Figs. 5(f) and 5(g)] However, electron-phonon coupling in the vicinity of $\mathbf{q}=(0.95,0,0)$ is much stronger for the interband transition than for the intraband transition. As a result of the strong electron-phonon coupling, the interband nesting peak that is only a factor of 2 stronger than the susceptibility at other wave vectors makes a dominant contribution to the phonon self-energy. Furthermore, any contribution to the phonon self-energy that does not have a strong $\mathbf{q}$ dependence would only influence the overall dispersion and cannot be responsible for the dispersion dip near a specific $\mathbf{q}$. Thus the phonon anomaly at $\mathbf{q}=(0.95,0,0)$ is caused primarily by interband transitions between bands 1 and 2 with a minor contribution from interband transitions between bands 1 and 3.

The predicted linewidths for all phonons were too small to be observed in our experiments performed with relatively coarse energy resolution of 3 meV FWHM. It is not possible to measure them with improved energy resolution with the currently available instrumentation without counting several times longer, although it would be interesting to make a more precise comparison with the theoretical predictions.

V. DISCUSSION

The salient feature of the phonon anomalies in the cuprates is that they are not reproduced by the LDA.[23] However, in chromium the phonon dispersions calculated in LDA agree reasonably well with experiment [Figs. 3(c) and 3(d)]. LDA yields the correct wave vectors where the softening occurs but overestimates its magnitude, especially at $\mathbf{q}=(0.94,0,0)$ [Fig. 3(a)]. The reason may be that magnetic interactions not included in LDA blur the Fermi surface and suppress the phonon softening. We note that a $\mathbf{Q}$-resolution effect would greatly enhance the observed linewidth due to the averaging over a wide range of frequencies but this was not observed. Both the calculations and experiments agree that the maximum phonon softening near the H point occurs at the wave vector of the SDW and not at the zone boundary.

The question arises why LDA correctly predicts the phonon anomalies that are completely unexpected from the joint density of states shown in Fig. 4. The answer is that phonon renormalization in LDA includes not only purely electronic band-structure features but also the electron-phonon coupling strength. Since the observed phonon softening along $\mathbf{q}=(h,1-h,0)$ is not related to the features of the band structure, it must be caused by enhanced electron-phonon coupling alone. Our calculations for each intraband and interband process identified the enhancement of electron-phonon coupling for interband transitions between bands 1 and 2 as responsible for all observed phonon dispersion dips. We speculate that the appearance of the softening at the zone boundary is not a coincidence because the eigenvectors of these phonons have a high symmetry leading to a more efficient coupling to certain electronic states. More work is necessary to prove or disprove this point.

The anomaly at $\mathbf{Q}^{\pm}$ is very sensitive to numerical smearing of the electronic states and thus of the Fermi surface whereas the anomaly at the N point is not. In addition, the interband transitions between bands 1 and 2 have nesting at $\mathbf{Q}^{\pm}$ and not elsewhere. Thus Fermi-surface nesting plays a big role in the $\mathbf{Q}^{\pm}$ anomaly in addition to the $\mathbf{q}$ dependence of electron-phonon coupling whereas the other anomalies result from the $\mathbf{q}$ dependence of electron-phonon coupling alone.

Previous reports of similar effects in other compounds have been controversial. For example, phonon anomalies in several transition-metal carbides have been explained in the past in terms of a $\mathbf{q}$ dependence of the electron-phonon coupling,[3,4] however, Noffsinger *et al.*[5] have shown that phonon anomalies resembling those in Cr occur exactly at the nesting wave vector and are narrow in $\mathbf{q}$. In contrast, phonon softening that was not associated with nesting was much broader in $\mathbf{q}$.

An enhancement of the electron-phonon matrix elements has also been proposed to explain a phonon anomaly in $NbSe_2$.[22,24] Therefore, our results may help to understand a wide range of materials. The current work also makes it clear that the possibility of electron-phonon coupling enhanced by electronic correlations as opposed to a "hidden" Fermi-surface nesting or collective modes should be seriously considered as an explanation of the phonon anomalies in the cuprates and other classes of materials. In contrast with Cr, the LDA fails to account for most phonon anomalies in the cuprates.[23] Thus an understanding of the giant bond-stretching phonon anomaly[25] within this framework would require an enhancement of the electron-phonon coupling beyond LDA, e.g., by electronic correlations.

ACKNOWLEDGMENT

The authors thank L. Pintschovius and W. Reichardt for held with model calculations and K. Machida for valuable feedback on the first version of the manuscript.

[1] W. Kohn, Phys. Rev. Lett. **2**, 393 (1959).
[2] B. Renker, L. Pintschovius, W. Gläser, H. Rietschel, R. Comès, L. Liebert, and W. Drexel, Phys. Rev. Lett. **32**, 836 (1974).
[3] H. G. Smith and W. Gläser, Phys. Rev. Lett. **25**, 1611 (1970).
[4] W. Weber, Phys. Rev. B **8**, 5082 (1973).
[5] J. Noffsinger, F. Giustino, S. G. Louie, and M. L. Cohen, Phys. Rev. B **77**, 180507 (2008).
[6] L. Pintschovius, Phys. Status Solidi B **242**, 30 (2005); D. Reznik, *ibid.* **2010**, 523549 (2010).
[7] W. M. Lomer, Proc. Phys. Soc. London **80**, 489 (1962).
[8] R. S. Fishman and S. H. Liu, Phys. Rev. Lett. **76**, 2398 (1996).
[9] H. Hiraka, Y. Endoh, P. Böni, M. Fujita, K. Yamada, and G. Shirane, Phys. Rev. B **67**, 064423 (2003).
[10] H. Hiraka, P. Böni, K. Yamada, S. Park, S-.H. Lee, and G. Shirane, Phys. Rev. B **70**, 144413 (2004).
[11] J. P. Hill, G. Helgesen, and D. Gibbs, Phys. Rev. B **51**, 10336 (1995).
[12] Y. Tsunoda, M. Mori, N. Kunitomi, Y. Teraoka, and J. Kanamori, Solid State Commun. **14**, 287 (1974).
[13] R. Pynn, W. Press, S. M. Shapiro, and S. A. Werner, Phys. Rev. B **13**, 295 (1976).
[14] M. Mori and Y. Tsunoda, J. Phys.: Condens. Matter **5**, L77 (1993).
[15] W. M. Shaw and L. D. Muhlestein, Phys. Rev. B **4**, 969 (1971).
[16] J. Trampenau, W. Petry, and C. Herzig, Phys. Rev. B **47**, 3132 (1993).
[17] S. G. Louie, K.-M. Ho, and M. L. Cohen, Phys. Rev. B **19**, 1774 (1979).
[18] B. Meyer, C. Elsässer, F. Lechermann, and M. Fähnle, FORTRAN90 Program for mixed-basis pseudopotential calculations for crystals, Max-Planck-Institut für Metallforschung, Stuttgart (unpublished).
[19] R. Heid and K.-P. Bohnen, Phys. Rev. B **60**, R3709 (1999).
[20] D. Vanderbilt, Phys. Rev. B **32**, 8412 (1985).
[21] J. P. Perdew and Y. Wang, Phys. Rev. B **45**, 13244 (1992).
[22] M. D. Johannes and I. I. Mazin, Phys. Rev. B **77**, 165135 (2008).
[23] D. Reznik, G. Sangiovanni, O. Gunnarsson, and T. P. Devereaux, Nature (London) **455**, E6 (2008).
[24] D. E. Moncton, J. D. Axe, and F. J. DiSalvo, Phys. Rev. B **16**, 801 (1977).
[25] D. Reznik, L. Pintschovius, M. Ito, S. Iikubo, M. Sato, H. Goka, M. Fujita, K. Yamada, G. D. Gum, and J. M. Tranquada, Nature (London) **440**, 1170 (2006).